IEEE Access
Multidisciplinary ⋮ Rapid Review ⋮ Open Access Journal

Received September 19, 2020, accepted October 12, 2020, date of publication October 26, 2020, date of current version November 9, 2020.

Digital Object Identifier 10.1109/ACCESS.2020.3033509

Electromagnetic and Levitation Characteristics of a High-Temperature Superconducting Bulk Above an Electromagnet Guideway

CHAOQUN ZHAO[1], MARK D. AINSLIE[2], (Senior Member, IEEE), AND YING XIN[1], (Senior Member, IEEE)

[1]School of Electrical and Information Engineering, Tianjin University, Tianjin 300072, China
[2]Bulk Superconductivity Group, Department of Engineering, University of Cambridge, Cambridge CB2 1PZ, U.K.

Corresponding author: Ying Xin (yingxin@tju.edu.cn)

This work was supported in part by the National Natural Science Foundation of China under Grant 51677131, and in part by the Engineering and Physical Sciences Research Council under Grant EP/P020313/1. All data are provided in full in the results section of this paper.

ABSTRACT An electromagnet guideway unit (EMGU) that can form an electromagnet guideway (EMG) with only a small gap, or even no gap, between multiple EMGUs was designed. The magnetic characteristics of such EMGU(s), including the homogeneity of the magnetic field along the EMGU(s) and the transverse magnetic field distribution were first investigated. As expected, the EMGU(s) can provide a homogeneous magnetic field in order to levitate bulk superconductors. Simulation results from an EMGU model implemented in COMSOL Multiphysics were verified using experimentally measured data, which indicated the established model can be used for further study and analysis. Next, the levitation characteristics of a high-temperature superconducting (HTS) bulk above the EMGU, including the levitation force acting on HTS bulk due to its interaction with the EMGU, as well as the stability of the bulk when experiencing a lateral disturbance and when varying the current of the EMGU, were investigated through experiment and simulation. The behavior of the levitation force during re-magnetization of the EMGU indicated that a larger re-magnetizing current is needed to suppress the internal magnetic field (trapped field) obtained from the pre-magnetization process, thereby providing a repulsive force to the superconductor. The stability study showed that the HTS maglev system with an EMGU with adjustable current can not only deal with a reduction of the levitation force but can also increase the restoring force when the superconductor is disturbed laterally. Finally, in order to clarify the mechanism of these levitation characteristics, the internal electromagnetic characteristics of the HTS bulk were analyzed using a 2D model.

INDEX TERMS HTS maglev, electromagnet guideway, levitation force, guidance force, stability, magnetization, HTS modeling.

I. INTRODUCTION

Electromagnetic interactions play a key role in magnetic levitation systems. A high-temperature superconducting (HTS) maglev system normally uses a permanent magnet (PM) as the magnetic field source [1]–[5]. HTS maglev vehicles above a permanent magnet guideway (PMG) have also been developed and investigated in the pursuit of HTS maglev operation [6]–[9]. There have been many developments related to maglev technology starting from fundamental studies on HTS bulks above PMs [10]. To assess the performance of an HTS-PM maglev system, the levitation characteristics of such systems, including magnetic field distributions generated by various PM arrangements [11]–[13], levitation force and guidance force [14]–[19], and stability [15], [20]–[22] have been investigated in numerous studies. These characteristics are strongly related to the electromagnetic interactions between the HTS and the PM.

However, there has been little work investigating the interaction between an electromagnetic guideway (EMG) and HTS bulks. HTS maglev using an EMG will reduce the resources required, especially if the guideway is installed over long distances. In contrast to a PM-based system, the attraction of ferromagnetic materials is not an issue for the EMG

The associate editor coordinating the review of this manuscript and approving it for publication was Wei Xu.

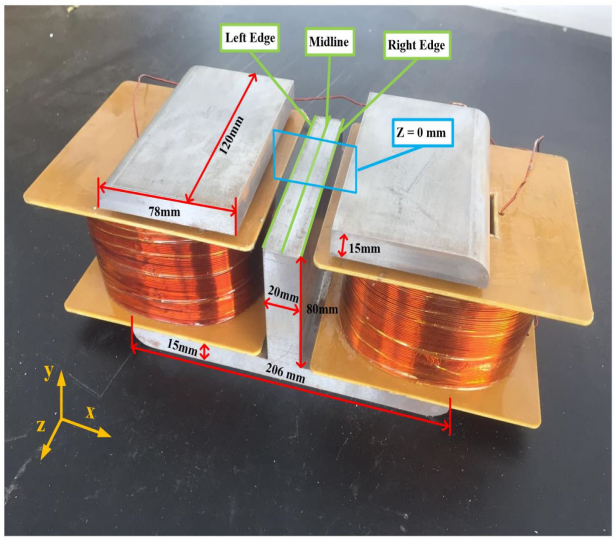

FIGURE 1. Structure and specifications of the EMGU investigated in this work.

when it is not energized, which increases the convenience of maintenance. Additionally, the magnetic flux density of the magnet can be varied by adjusting the current of the EMG for different loads. In principle, the EMG also can adopt a segmented instant excitation (SIE) mode to realize a minimum levitation power loss when the train body moves above the EMG, as well as sufficient levitation force and guidance force. In other words, exciting the EMGUs in the area where the train body is currently located and then powering them off once the train body has passed by [23], [24]. The EMG can be formed by the arrangement of multiple electromagnetic guideway units (EMGUs). Therefore, the fundamental characteristics of an HTS bulk above an EMGU for HTS maglev are investigated in detail in this work.

For this study, an EMGU that allows the formation of an EMG with small or no gap between EMGUs was designed [24]–[27]. The levitation force vibrates if the superconductor experiences an inhomogeneous magnetic field along the guideway [28] and the levitation characteristics and performance are closely related to the transverse magnetic field. Therefore, the longitudinal magnetic field homogeneity generated by a single EMGU, and two EMGUs, and the transverse magnetic field distribution of the EMGU at $z = 0$ mm (see Fig. 1) are investigated. The levitation force of the HTS bulk generated by the EMGU's pre-magnetization and re-magnetization are investigated through experiment and simulation. The levitation force attenuates [17], [22] and a restoring force (guidance force) is needed when the bulk is disturbed laterally. Hence, the maglev stability of an HTS bulk experiencing a lateral disturbance and when varying the current of the EMGU is also investigated through experiment and simulation. These levitation characteristics are simulated using a 3D finite-element model implemented in COMSOL Multiphysics. Additionally, the electromagnetic characteristics inside the bulk obtained from a 2D model are analyzed in order to understand these levitation characteristics better.

II. EXPERIMENTAL SETUP

The structure and specifications of the experimental EMGU setup are shown in Fig. 1. It consists of two multi-turn coils and an iron core. The two side posts are respectively wound with the two coils that are connected in series and energized by a DC power supply. The coils are wound by insulated copper wire of diameter 1.08 mm. The number of turns of each coil is 1692. The longitudinal and transverse directions of the EMGU are the z-axis and x-axis directions, respectively. The coils of the EMGU do not extend beyond the frame of the iron core along the z-axis, such that the EMGUs can be arranged without a gap. Fig. 2 shows our measurement system with a 3D sliding platform and force sensors. The precision of the vertical and horizontal force sensors is $\leq \pm 0.017\%$ FS and $\leq \pm 0.3\%$ FS, respectively. The HTS bulk, fixed at the bottom of the liquid nitrogen vessel, is a cylindrical melt-textured YBCO bulk of diameter of 30 mm and thickness of 15 mm, which was provided by the General Research Institute for Nonferrous Metals. The reaction force acting on the EMGU is the levitation force of the HTS bulk, and the horizontal force is obtained when EMGU is moved horizontally, which is detailed in [29]. The bulk is immersed in liquid nitrogen throughout the experiments. The following sections detail each of the experiments.

A. MAGNETIC FIELD HOMOGENEITY AND TRANSVERSE MAGNETIC FIELD DISTRIBUTION

The magnetic field homogeneity of a single EMGU was first investigated. The EMGU was energized with different DC currents (1, 2 and 3 A) and the y component of the magnetic field flux density (B_y) at different heights (2, 5 and 8 mm) above the midline, left edge and right edge (see Fig. 1) were measured.

In addition, B_y of the transverse magnetic field, at $z = 0$ mm (see Fig. 1), at 2 mm above the guideway surface for different excitation currents (1, 2 and 3 A), as well as at different heights (2, 5 and 8 mm) above guideway surface for a current of 3 A, was measured.

B. LEVITATION FORCE DUE TO EMGU PRE-MAGNETIZATION AND RE-MAGNETIZATION

This experiment consists of a pre-magnetization process and a re-magnetization process. In the pre-magnetization process, the HTS bulk is first cooled by liquid nitrogen at a particular cooling height in the presence of the magnetic field generated by the EMGU with a DC current I_{EMGU}, which corresponds to a field-cooled (FC) magnetisation method. The current is then reduced to 0.01 A and some magnetic field (the so-called trapped field) remains inside the YBCO bulk. After 5 seconds, the re-magnetization process is initiated: the current is increased to 3.51 A at a rate of 0.1 A/s, which is similar to a zero-field-cooled (ZFC) magnetisation method.

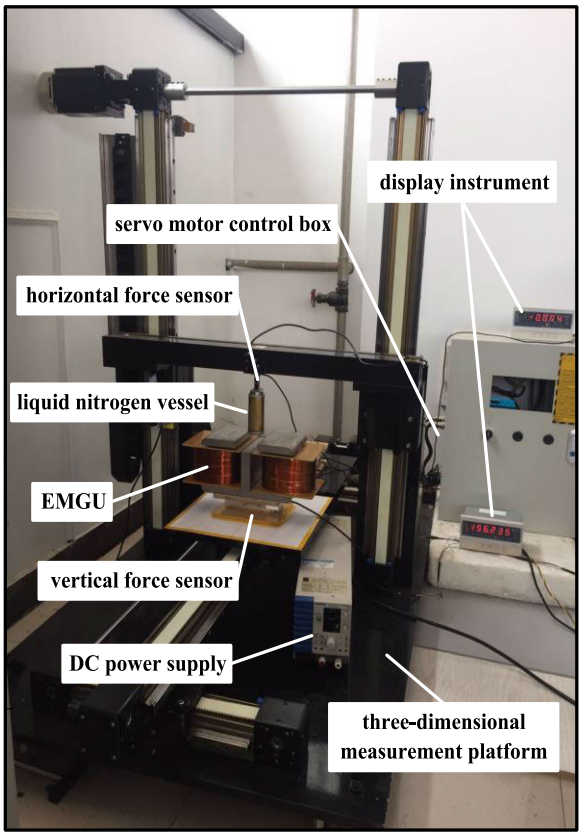

FIGURE 2. The force measurement system for HTS maglev.

The levitation force acting on the HTS bulk is recorded during the re-magnetization process. The experiments are carried out at different cooling heights (2, 5 and 8 mm) above the guideway surface with different I_{EMGU} (1, 2 and 3 A).

C. STABILITY STUDY WHEN VARYING EMGU CURRENT

The stability study is carried out as follows. Firstly, the bulk at 5 mm above the guideway surface is cooled by liquid nitrogen in the presence of the magnetic field generated by the EMGU with different DC currents, I_{EMGU}. The HTS bulk is then moved from $x = 0$ mm to $x = 6$ mm at a speed of 0.5 mm/s. A 45-second relaxation period follows the 6 mm lateral motion. After the relaxation process, the current flowing in the EMGU was increased from I_{EMGU} to 3.5 A. Finally, after another 45-second relaxation period the power was turned off. The levitation force and guidance force are recorded after the lateral movement. This study is carried out with different I_{EMGU} (1, 2, and 3 A).

III. NUMERICAL MODEL

A. HTS-EMGU MODEL

Numerical modeling is a powerful and cost-effective tool to better analyse and optimize the HTS maglev system. Finite-element models based on the $\boldsymbol{H}$-formulation have been applied to analyse various problems related to HTS materials [16], [30]–[37]. In this work, the HTS-EMGU maglev model is built in COMSOL Multiphysics using a segregated $\boldsymbol{H}$-formulation method, based on unidirectional coupling between the EMGU model and the HTS model [16], [36]–[38]. The coupling between these two models is achieved by applying the sum of the external magnetic field from the EMGU and the self-field of the HTS bulk on the outer boundaries of the HTS model. This particular method of modeling the system is extremely useful as it avoids the need for a single, time-dependent finite-element model of the entire system and the use of a moving mesh. There is also a significant reduction in the number of mesh elements required in the time-dependent, highly nonlinear HTS model. The static external magnetic field is obtained from the EMGU model. The self-field is generated by the induced current inside the HTS bulk and is obtained from the HTS model by numerical integration of the Biot-Savart law.

The EMGU model based on the actual geometry of the experimental setup was built in COMSOL Multiphysics. The EMGU model is a magnetostatic finite-element model of the EMGU energized by a DC current, which is used for the analysis of the magnetic field generated by the EMGU and the simulation results of the magnetic field (longitudinal and transverse magnetic fields) were compared with measured data. Meanwhile, a 3D model consisting of two EMGUs arranged in a line with different gaps (0.5 and 2 mm) between them was established to investigate the homogeneity of the longitudinal magnetic field generated by the two EMGUs. The magnetic field (MF) interface in COMSOL's AC/DC module is used to compute the external field generated by the EMGU. The ***Coil*** node in the MF interface is used to specify the type of coil and its parameters. The "Numeric" coil type is used and the assumed parameters of the coil, including "coil excitation", "number of turns", and "coil wire conductivity" (copper at room temperature), are listed in Table 1.

The HTS model is also a finite-element model consisting of an HTS subdomain surrounded by a thin air subdomain. It is time-dependent and modelled using the $\boldsymbol{H}$-formulation. Neglecting the displacement current, Ampere's law gives:

$$\nabla \times \boldsymbol{H} = \boldsymbol{J} \tag{1}$$

where $\boldsymbol{H}$ is the magnetic field strength and $\boldsymbol{J}$ is the current density. According to Ohm's law:

$$\boldsymbol{E} = \rho \boldsymbol{J} \tag{2}$$

where $\boldsymbol{E}$ is the electric field and ρ is the resistivity. The nonlinear resistivity of the superconductor is characterized by the E-J power law; thus, the resistivity of the HTS subdomain in the HTS model can be written as:

$$\rho = \frac{E_c}{J_c(\boldsymbol{B})} \left| \frac{\boldsymbol{J}}{J_c(\boldsymbol{B})} \right|^{n-1} \tag{3}$$

where E_c is critical current characteristic electric field and $J_C(\boldsymbol{B})$ is the field-dependent critical current density. The resistivity of the air subdomain is assumed simply as 1 Ωm.

TABLE 1. Assumed parameters for the EMGU and HTS models.

Symbol	Quantity	Value
E_c	Critical current characteristic electric field	1×10^{-4} V/m
B_0	HTS parameter, Kim model	0.37 T
n	HTS parameter, n value	21
J_{c0}	HTS parameter, Kim model	5×10^7 A/m^2
μ_0	Air/HTS permeability	$4\pi \times 10^{-7}$ H/m
N	Number of turns	1692
σ	Coil wire conductivity	6×10^7 S/m

According to Faraday's law:

$$\nabla \times \boldsymbol{E} = -\mu_0 \frac{\partial \boldsymbol{H}}{\partial t} \tag{4}$$

Substituting (1) and (2) into (4), the $\boldsymbol{H}$-formulation can be represented by the following form:

$$\nabla \times \rho(\nabla \times \boldsymbol{H}) = -\mu_0 \frac{\partial \boldsymbol{H}}{\partial t} \tag{5}$$

where μ_0 is the vacuum magnetic permeability. The general form, equation (5), can be solved by COMSOL Multiphysics. The HTS material here is an HTS bulk superconductor, and the field-dependence of J_c ($\boldsymbol{B}$) is characterized by an isotropic Kim-like model [39],

$$J_c(\boldsymbol{B}) = J_{c0} \frac{B_0}{|\boldsymbol{B}| + B_0} \tag{6}$$

where J_{c0} is the self-field critical current density and B_0 is a material parameter.

The displacement of the bulk is achieved by modifying the spatial external field generated in the reference frame of the EMGU model using displacement functions [37]. In order to simulate the variation of external field due to the adjustment of current in HTS model, we multiply the unit magnetic field (generated by a current of 1 A) by a time-varying function. Fig. 3 shows the time-varying function corresponding to $I_{EMGU} = 1$ A in the experiments in sections II.B and II.C, respectively. The reason for the shape of the time-varying function is explained in detail in section IV.A.

The force between the EMGU and HTS bulk can be calculated by

$$\boldsymbol{F} = \iiint_{\Omega_{sc}} \boldsymbol{B} \times \boldsymbol{J} dV \tag{7}$$

where Ω_{sc} is the HTS subdomain and dV is the differential volume. The levitation and guidance forces are further written as:

$$\begin{aligned} \boldsymbol{F}_{lev}(t) = & \iiint_{\Omega_{sc}} J_z(x', y', z', t) \cdot B_x(x', y', z', t) \\ & - J_x(x', y', z', t) \cdot B_z(x', y', z', t)\, dx'dy' \end{aligned} \tag{8}$$

$$\begin{aligned} \boldsymbol{F}_{gui}(t) = & \iiint_{\Omega_{sc}} J_y(x', y', z', t) \cdot B_z(x', y', z', t) \\ & - J_z(x', y', z', t) \cdot B_y(x', y', z', t)\, dx'dy' \end{aligned} \tag{9}$$

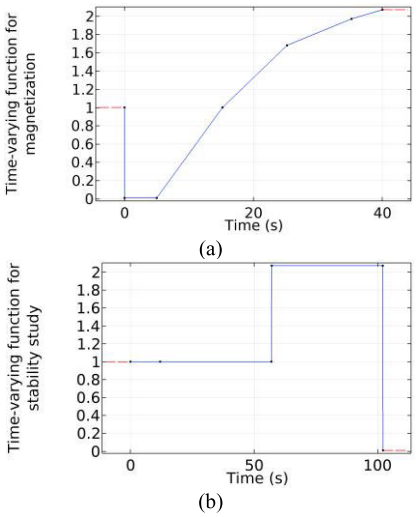

FIGURE 3. The time-varying function used in the HTS model for simulating (a) the re-magnetization process and (b) the stability study.

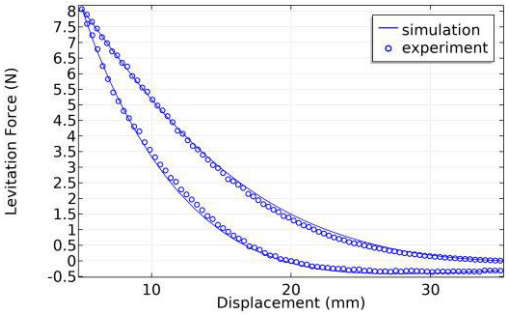

FIGURE 4. Model validation: levitation force for the ZFC process.

B. HTS-EMGU MODEL CALIBRATION

The 3D numerical model is used in the calibration. For the calibration of the model, the common practice is to use the maximum levitation force obtained from a zero-field cooling (ZFC) process [40]–[42]. This process involves first cooling the HTS bulk at 35 mm above the center of the EMGU in the presence of the magnetic field generated by the EMGU with a current of 3 A. Afterwards, the bulk is moved vertically to 5 mm at a rate of 1 mm/s and then moved vertically back to the initial position. In order to ensure that the maximum simulated levitation force during the ZFC process is equal to the measured value (see Fig. 4), J_{c0} is set to $5 \times 10^7 A/m^2$. The other HTS bulk parameters are set to commonly used values. The parameters assumed for this model are listed in Table 1.

IV. RESULTS AND DISCUSSION

A. MAGNETIC FIELD HOMOGENEITY AND TRANSVERSE MAGNETIC FIELD DISTRIBUTION

Due to symmetry of the magnetic field distribution along the guideway, B_y from the measured data (symbols) and simulation results (lines) for half the EMGU guideway are shown in Fig. 5. The measured data shows that B_y above the midline is lower than that of the left and right edges at heights

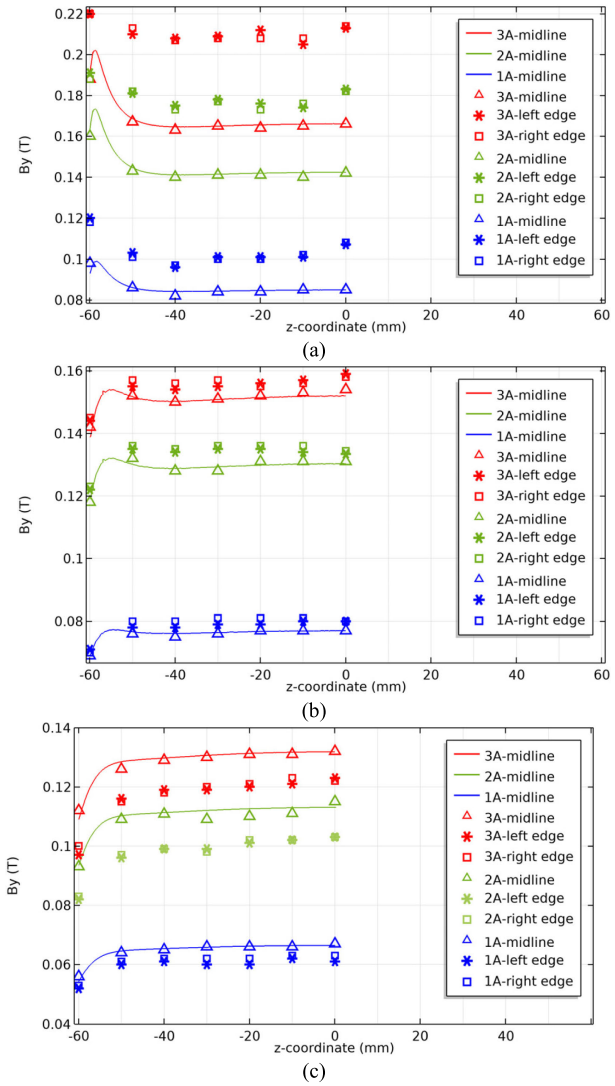

FIGURE 5. B_y of the EMGU at (a) 2 mm, (b) 5 mm and (c) 8mm above the midline and left and right edges with different excitation currents.

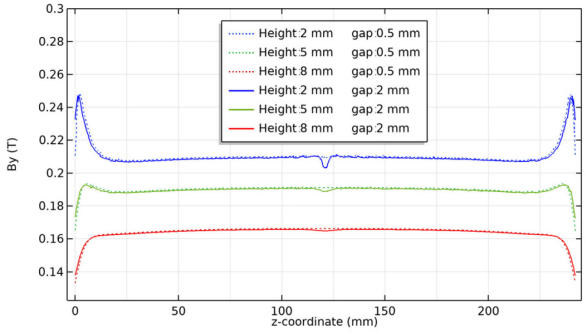

FIGURE 6. B_y of two EMGUs at different heights with different gaps (0.5 and 2 mm) between them and a current of 3 A.

of 2 and 5 mm, as shown in Figs. 5(a) and 5(b). However, as the height reaches 8 mm, the values of B_y above the midline are higher than both edges, as shown in Fig. 5(c). The longitudinal magnetic field generated by the EMGU is homogeneous except for its two ends. In addition, the simulation results

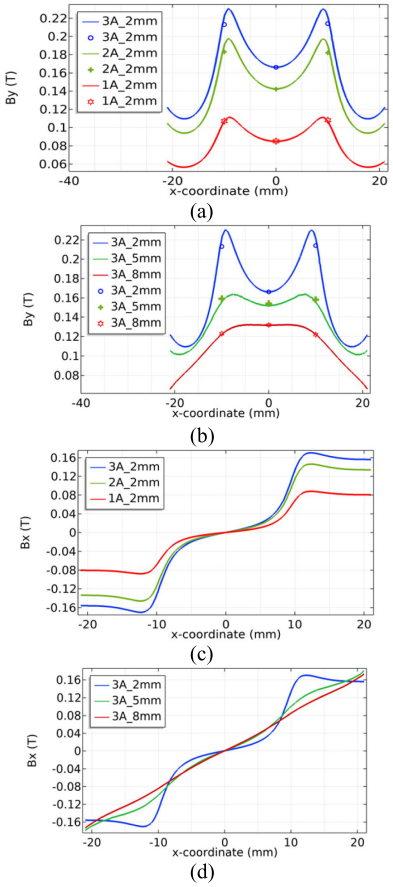

FIGURE 7. Transverse (a) B_y and (c) B_x for different excitation currents at a height of 2 mm. Transverse (b) B_y and (d) B_x for an excitation current of 3 A at different heights.

of B_y above the midline are consistent with the measured data, which indicates that the model is reliable for further study and analysis.

Fig. 6 presents the simulation results of B_y generated by a current of 3 A at different heights with different gaps (0.5 and 2 mm) between two EMGUs. The homogeneity of B_y along the two EMGUs is good. B_y has a larger fluctuation for the gap of 2 mm than for 0.5 mm. It indicates that the larger the gap, the more obvious the fluctuation. Therefore, it is desirable that the EMGUs should be arranged as close as possible for minimizing fluctuation of the magnetic field at the gap. It is also found that the fluctuation of B_y is subtle at a height of 2 mm or higher above the EMGUs' surface, at which a longitudinal homogeneous magnetic field can be provided to the superconductor for stable operation.

We only investigated the EMGU's magnetic field distribution at $z = 0$ mm (see Fig. 1) as a representative case because of the longitudinal homogenous magnetic field. As shown in Figs. 7(a) and 7(b), the measured values (symbols) and simulation results (lines) of B_y show excellent agreement. The shape of the B_y distributions with different currents at a height of 2 mm are identical and the values of B_y at $x = 0$ mm are smaller than that near the guideway edges, which can

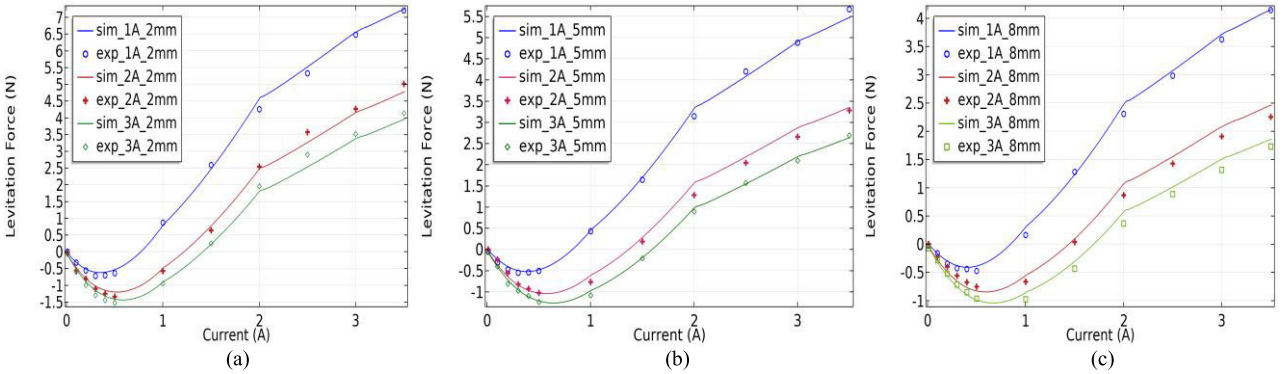

FIGURE 8. Levitation force versus re-magnetizing current with different I_{EMGU} at cooling heights of (a) 2 mm, (b) 5 mm and (c) 8 mm.

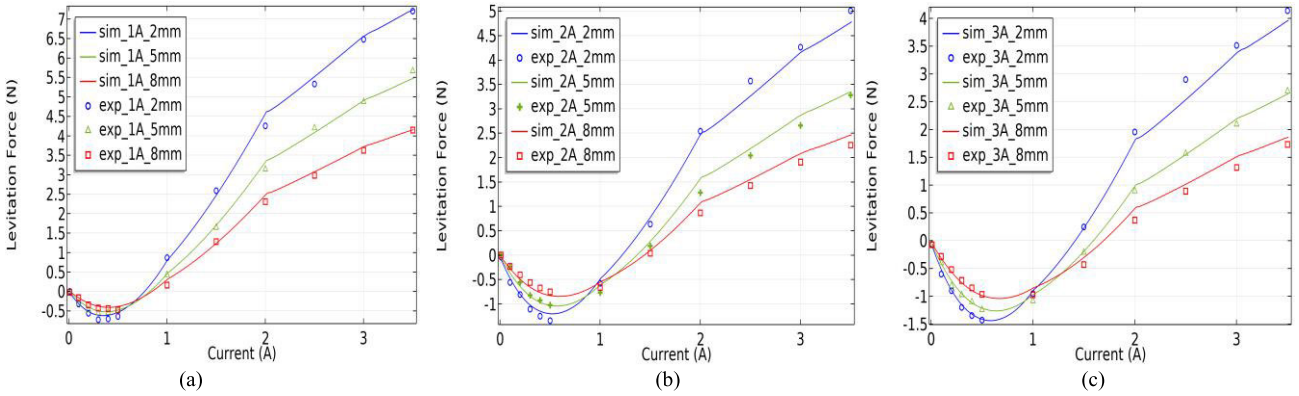

FIGURE 9. Levitation force versus re-magnetizing current at cooling heights of 2, 5 and 8 mm for (a) $I_{EMGU} = 1$ A, (b) $I_{EMGU} = 2$ A and (c) $I_{EMGU} = 3$ A.

be seen from Fig. 7(a). However, Fig. 7(b) presents different distributions of B_y with a current of 3 A at different heights. The magnetic field distribution from $x = -10$ mm to $x = 10$ mm changes from a concave shape to a convex one as the height increases. Figs. 7(c) and 7(d) present simulation results for B_x, which has a similar regularity as B_y.

From the longitudinal magnetic field (Fig. 5) or the transverse magnetic field (Figs. 7(a) and 7(b)), it can be concluded that if the magnetic field generated by current of 1 A is normalized to 1, the magnetic fields generated by 2 and 3 A are 1.68 and 1.97, respectively, which indicates the magnetic field (external field) increases nonlinearly with the increase of the current. Thus, the nonlinear relationship between the magnetic field and current can be approximated as a piecewise linear function. Therefore, the time-varying function in Fig. 3(a) – a multiplying unit external magnetic field – is used to simulate the variation of the magnetic field during the magnetization process in the HTS model. Similarly, the time-varying function used when simulating the stability study is shown in Fig. 3(b). The unit static external field is obtained from the EMGU model and the product of the time-varying function and the unit static external field as a varying external field is applied on the outer boundary of the HTS model in the simulation.

B. LEVITATION FORCE DUE TO EMGU PRE-MAGNETIZATION AND RE-MAGNETIZATION

Figs. 8 and 9 present the relationship between the levitation force and the current during the re-magnetization process. The experimental results (symbols) agree well with simulated results (lines). The force acting on the YBCO bulk changes from an attractive force (negative value) to a repulsive force (positive value) as the re-magnetizing current increases. The levitation force during the re-magnetization process first increases in the form of attraction, then decreases in the form of attraction, and finally increases in the form of a repulsive force. This is because the induced current interacts with the magnetic field inside the superconductor. The current, $I_{pre\text{-}ind}$, was induced within the YBCO bulk when the current of the EMGU reduced to 0.01 A, which resulted in some magnetic field to remain (trapped field). The shielding current, $I_{re\text{-}ind}$, opposite to $I_{pre\text{-}ind}$ is induced within the bulk when the re-magnetizing current of the EMGU starts to increase. The mechanism of the levitation characteristics will be analysed in section IV.D through 2D simulated results.

As can be seen from Fig. 8, the larger I_{EMGU} is, the larger the re-magnetizing current needed to generate the levitation force. This is because the larger I_{EMGU} results in more trapped magnetic field once the current decreases to 0.01 A.

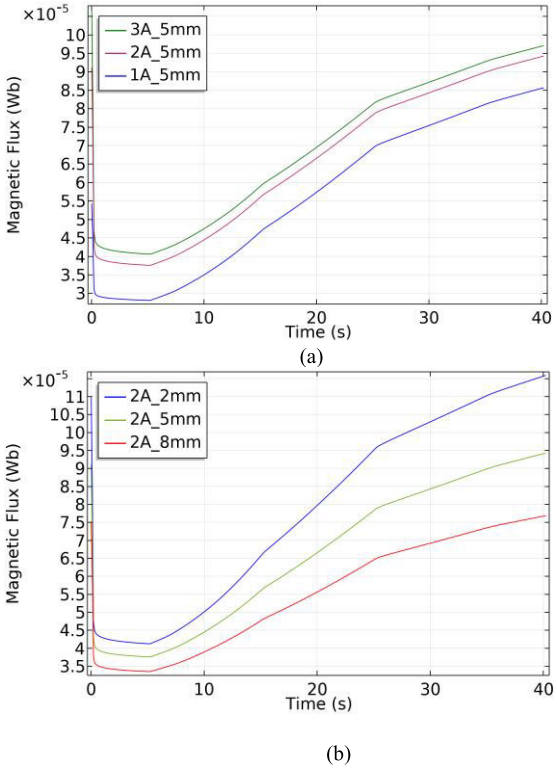

FIGURE 10. Magnetic flux of the bottom surface of the bulk (a) at a height of 5 mm with different I_{EMGU} and (b) at different heights with $I_{EMGU} = 2$ A.

We can use the magnetic flux of the superconductor's bottom surface at a current of 0.01 A to describe the trapped magnetic field. Fig. 10(a) shows the simulated magnetic flux of the bottom surface for a height of 5 mm with different I_{EMGU}, which corresponds to Fig. 8(b). As can be seen from Fig. 10(a), the larger I_{EMGU} is, the more magnetic flux when the current decreased to 0.01 A, the more trapped field there is.

From Fig. 9, the lower the cooling height is, the more trapped flux there is, and the larger the negative force in the initial stage of the re-magnetization process. However, the lower the cooling height is, the faster the magnetic field change experienced by YBCO bulk is for the same increasing re-magnetizing current, which can be seen from Fig. 10(b). Fig. 10(b) shows the simulated magnetic flux of the bottom surface for $I_{EMGU} = 2$ A at different heights, which corresponds to Fig. 9(b). Therefore, a faster increase of $I_{re\text{-}ind}$ within the bulk due to the faster magnetic field change results in a more rapid increase in the levitation force. Consequently, although the levitation force started with a stronger negative force due to more trapped field at a lower cooling height, it increases faster and generates a stronger repulsive force with increasing re-magnetizing current.

C. STABILITY STUDY OF HTS-EMGU

Fig. 11 shows the levitation force, guidance force and magnetic flux through the bottom surface of the bulk versus time for different I_{EMGU} (1, 2 and 3 A). The experimental results for the levitation and guidance forces show excellent agreement with the simulation results. The larger I_{EMGU} is, the guidance force increases faster with the offset increasing, which can be seen from Fig. 11(b). The guidance force for

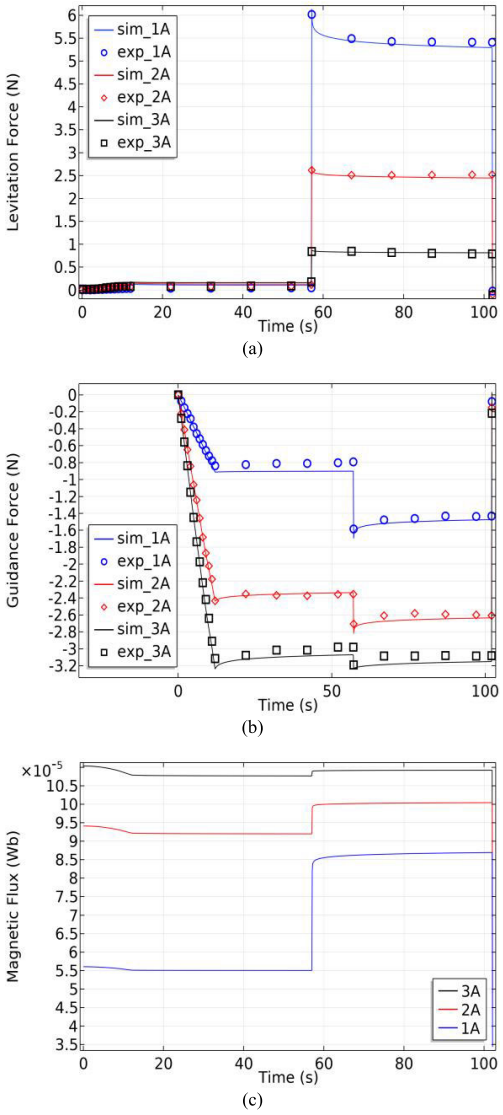

FIGURE 11. (a) Levitation force (b) guidance force and (c) magnetic flux of the bottom surface of the bulk versus time for different I_{EMGU}.

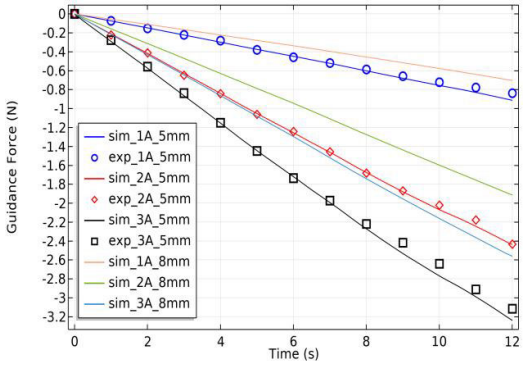

FIGURE 12. Comparative analysis of the guidance force at different heights.

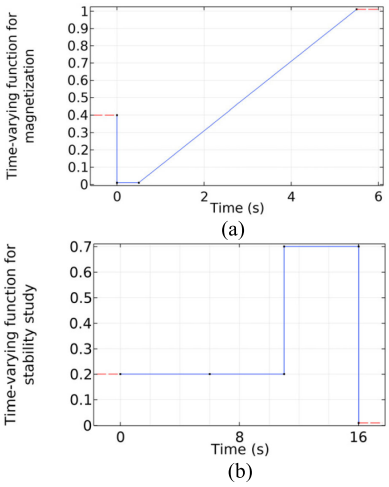

FIGURE 13. Time-varying function for (a) the magnetization process and (b) the stability study in the 2D simulation.

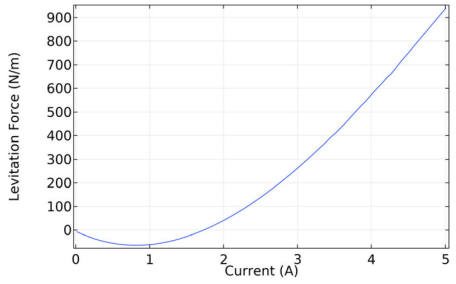

FIGURE 14. The levitation force generated by re-magnetization of the EMGU.

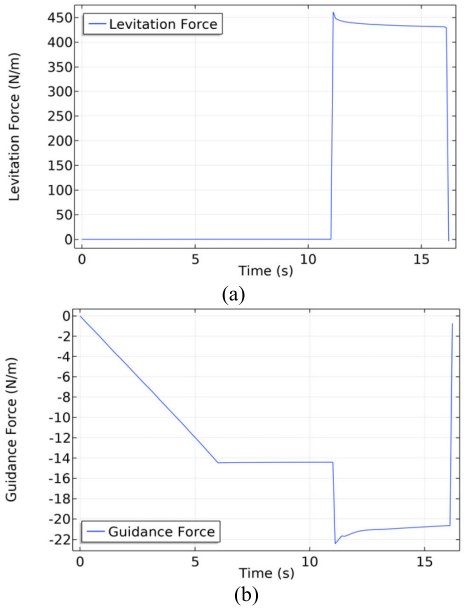

FIGURE 15. (a) Levitation force and (b) guidance force for the stability study.

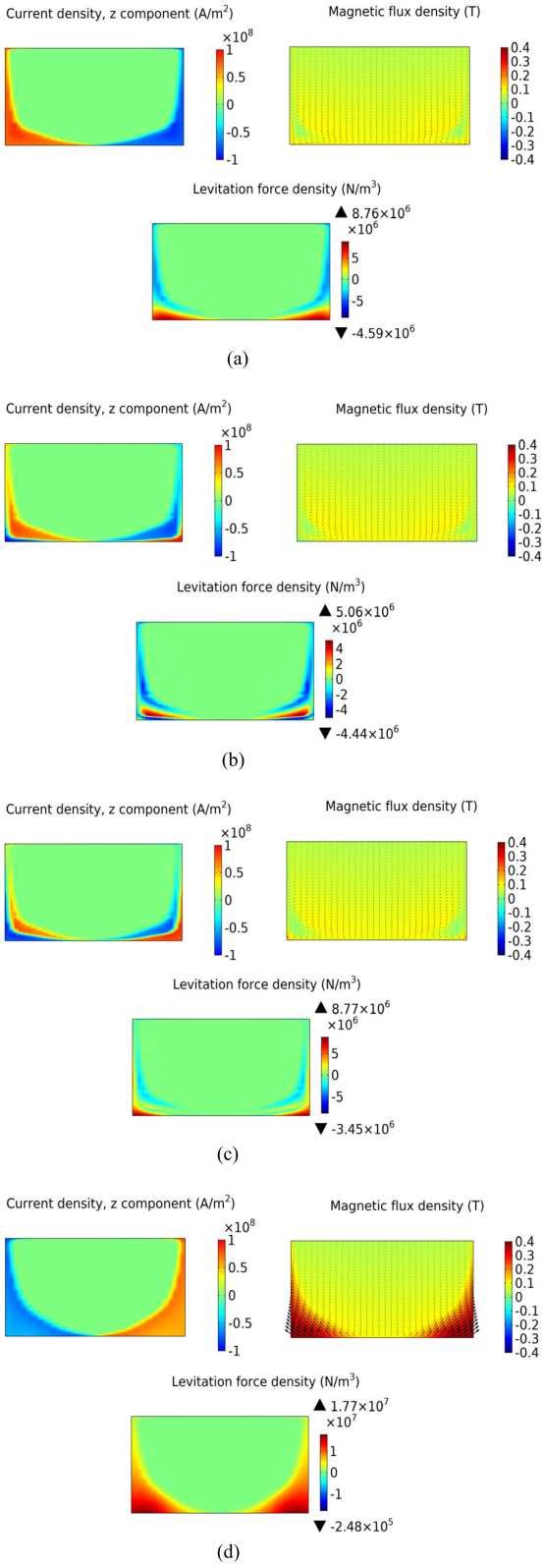

FIGURE 16. The electromagnetic characteristics during the EMGU's re-magnetization process at (a) initial (b) lowest (c) zero and (d) maximum positions of the levitation force.

larger I_{EMGU} enables the YBCO bulk to return to its original position more easily (x = 0 mm). During the relaxation time, the levitation force and guidance force hardly change. It can be seen from Fig. 11(c) that the trends for the levitation and guidance forces are consistent with that of the magnetic

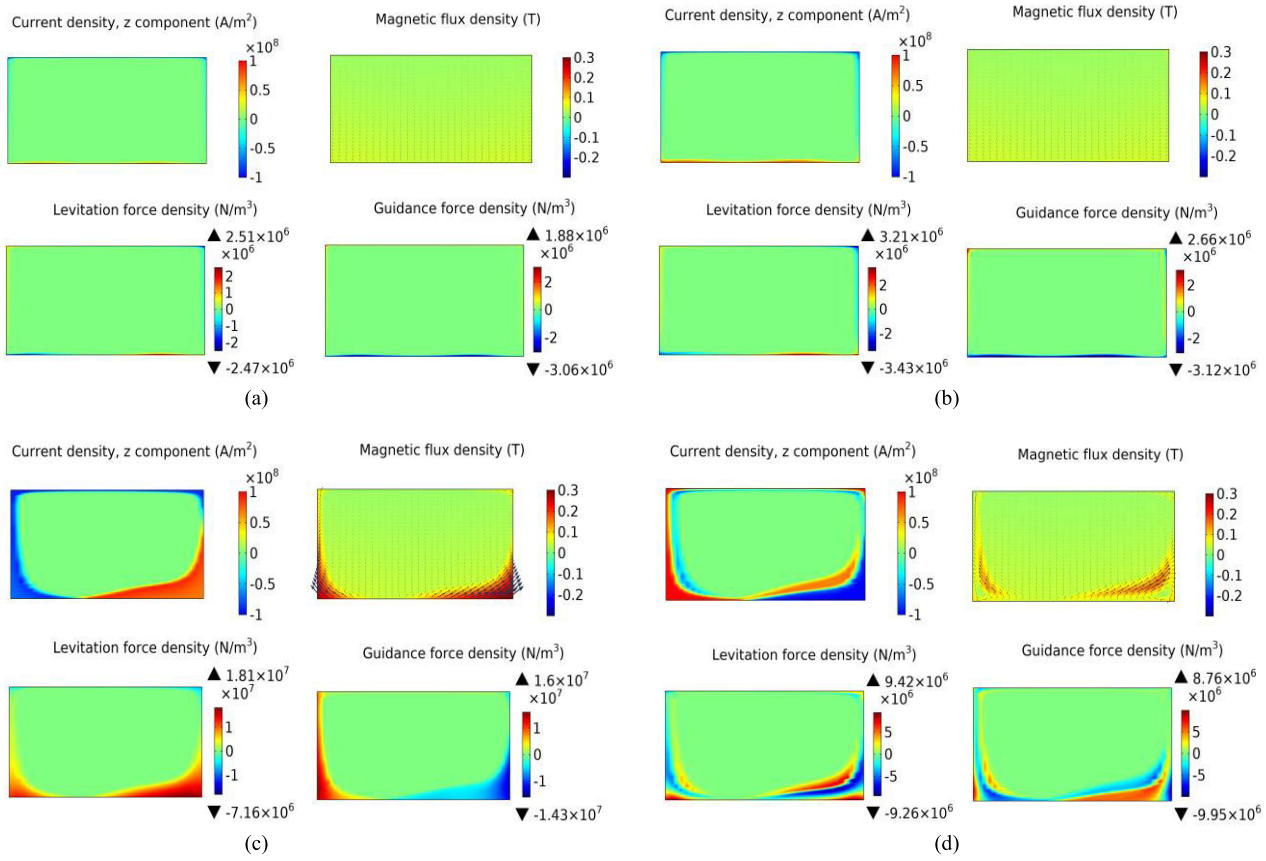

FIGURE 17. Stability study of HTS-EMGU by adjusting coil current at (a) 3s (b) 6s (c) 11s and (d) 16s.

flux. It is worth noting that both the levitation and guidance forces increased after the current was increased, which could enhance the stability of HTS maglev system using the EMGU. This is because the levitation force decreases when the superconductor experiences reciprocating lateral movements [21], [24]. Meanwhile, a restoring force (guidance force) is needed when the superconductor is moved laterally. It just so happens that the HTS maglev with the EMGU can increase the levitation and restoring forces at the same time. The levitation and guidance forces are negative when the current is decreased to 0.01 A. The larger the I_{EMGU} is, the larger the negative levitation and guidance forces are. These characteristics obtained from this stability study are a result of the electromagnetic interaction. The mechanism of these characteristics is presented in the following section (IV.D) is described using 2D simulation results.

The guidance force for the 6 mm lateral movement at a height of 8 mm above the guideway with different I_{EMGU} (1, 2, and 3 A) was simulated and the simulation results were compared with that for a height of 5 mm. Fig. 12 shows the guidance force at heights of 5 and 8 mm for different I_{EMGU} (1, 2 and 3 A). The simulated guidance force for ''2A_5mm'' is larger than that of ''2A_8mm'' because the field-cooling occurs at a lower height. However, although the height of ''2A_5mm'' is lower than that of ''3A_8mm'', the guidance forces are similar, which indicates the guidance force can be compensated by increasing the current. Therefore, the guidance force of superconductor can be enhanced dynamically with the EMGU.

D. MECHANISM OF LEVITATION CHARACTERISTICS

A 2D model having mostly the same parameters as the 3D model was also built and used here to clarify the mechanism of the levitation characteristics (levitation force due to EMGU magnetization and stability of the HTS-EMGU by adjusting the coil current) quickly and efficiently. The parameters used here are same as those given in Table 1, except that a higher value of $J_{c0} = 1\times10^8 A/m^2$ is used to greater emphasise the interaction. The external magnetic field generated by a current of 5 A was firstly obtained from a 2D EMGU model. The external magnetic field generated by 5 A is used in a normalization process similar to Section IV.A such that multiplying by a time-varying function achieves the variation of magnetic field due to the adjustment of current in the 2D HTS model. The time-varying functions for simulating the magnetization process and used in the stability study are shown in Fig. 13.

The simulated levitation force due to re-magnetization of the EMGU and the stability of the HTS-EMGU when varying the coil current are shown in Figs. 14 and 15, respectively, which have the same trends as those obtained from the 3D model. These levitation characteristics resulted

from the electromagnetic characteristics inside the superconductor. The electromagnetic characteristics for several representative force values at the initial, lowest, zero and maximum positions (see Fig. 14) for the levitation force during the re-magnetization process are shown in Fig. 16. The behaviour of the levitation force is a result of the interaction between the induced current and the magnetic field, which can be calculated from equation (7). The induced current in Fig. 16(a) is $I_{pre\text{-}ind}$. $I_{re\text{-}ind}$ was induced at the bottom surface of superconductor underneath this $I_{pre\text{-}ind}$, which can be seen in Figs. 16 (b) and 16 (c). The magnitude and direction of the current and magnetic field inside the superconductor determine the magnitude and direction of the local forces in the superconductor, as described in equations (8) and (9). The superposition of these forces is responsible for the levitation force characteristic in Fig. 14 and a guidance force that is zero. Fig. 17 shows the electromagnetic characteristics at times t = 3, 6, 11 and 16 s for the stability study of the HTS-EMGU by regulating the current. Similarly, the behaviour of the forces in the stability study is also caused by internal electromagnetic properties, which the model allows us to visualise.

V. CONCLUSION

The designed EMGU can form an EMG (track) with a small gap, or even no gap, between linearly arranged EMGUs and provide a homogeneous longitudinal magnetic field for efficient levitation of a bulk superconductor. The longitudinal magnetic field of two EMGUs shows that the smaller the gap and higher the height, the more homogenous the longitudinal magnetic field is, but the magnetic field decreases as the height increases. When investigating the levitation force due to EMGU pre-magnetization and re-magnetization, it was found that a larger re-magnetizing current is needed for more trapped magnetic field (larger I_{EMGU} at lower cooling height) to provide the repulsive force for the bulk superconductor. When the bulk superconductor is moved laterally to a position, the HTS maglev system with the EMGU can not only deal with the reduction of the levitation force but also increase the guidance force to return the superconductor to an equilibrium position dynamically by increasing the current of the EMGU, which should enhance the stability of HTS maglev operation with an EMG.

A 3D model of the system based on a segregated $\boldsymbol{H}$-formulation finite-element method – that can simulate the dynamics of the system in a fast and efficient manner – has been built and validated by experimental results. A simplified 2D model was then used to visualize and clarify the details and mechanism of the levitation characteristics.

The electromagnetic characteristics inside superconductor resulted in the particular levitation characteristics above the EMGU and are related to the variation of the external magnetic field impinging on the bulk superconductor. This study investigated the fundamental research on the levitation characteristics of a YBCO bulk above EMGU, which lays a foundation for optimization of HTS maglev with an EMG. Using the established models, one can carry out detailed simulation studies on the levitation characteristics during the dynamic operation of an EMGU, including the motion and the electromagnetic properties of the bulk superconductor, in an accurate and efficient manner. This will aid the development of an appropriate SIE mode that can realize a minimum levitation power loss when the train body moves above the EMG, as well as sufficient levitation force and guidance force, in practical systems.

REFERENCES

[1] E. H. Brandt, "Levitation in physics," *Science*, vol. 243, no. 4889, pp. 349–355, Jan. 1989.
[2] J. R. Hull, "Superconducting bearings," *Superconductor Sci. Technol.*, vol. 13, no. 12, pp. R1–R15, May 1999.
[3] F. C. Moon, M. M. Yanoviak, and R. Ware, "Hysteretic levitation forces in superconducting ceramics," *Appl. Phys. Lett*, vol. 52, no. 18, p. 1534, Mar. 1988.
[4] Y. Tachi, N. Uemura, K. Sawa, Y. Iwasa, K. Nagashima, T. Otani, T. Miyamoto, M. Tomita, and M. Murakami, "Force measurements for levitated bulk superconductors," *Supercond. Sci. Technol.*, vol. 13, no. 6, p. 850, Jan. 2000.
[5] T. A. Coombs, A. Cansiz, and A. M. Campbell, "A superconducting thrust-bearing system for an energy storage flywheel," *Superconductor Sci. Technol.*, vol. 15, no. 5, p. 831, Apr. 2002.
[6] Z. Deng, W. Zhang, J. Zheng, Y. Ren, D. Jiang, X. Zheng, J. Zhang, P. Gao, Q. Lin, B. Song, and C. Deng, "A high-temperature superconducting maglev ring test line developed in Chengdu, China," *IEEE Trans. Appl. Supercond.*, vol. 26, no. 6, pp. 1–8, Sep. 2016.
[7] J. Wang, S. Wang, Y. Zeng, H. Huang, F. Luo, Z. Xu, Q. Tang, G. Lin, C. Zhang, Z. Ren, and G. Zhao, "The first man-loading high temperature superconducting maglev test vehicle in the world," *Phys. C, Supercond. Appl.*, vols. 378–381, pp. 809–814, Oct. 2002.
[8] L. Schultz, O. D. Haas, P. Verges, C. Beyer, S. Rohlig, H. Olsen, L. Kuhn, D. Berger, U. Noteboom, and U. Funk, "Superconductively levitated transport system—The SupraTrans project," *IEEE Trans. Appiled Supercond.*, vol. 15, no. 2, pp. 2301–2305, Jun. 2005.
[9] G. G. Sotelo, R. A. H. de Oliveira, F. S. Costa, D. H. N. Dias, R. de Andrade, and R. M. Stephan, "A full scale superconducting magnetic levitation (MagLev) vehicle operational line," *IEEE Trans. Appl. Supercond.*, vol. 25, no. 3, pp. 1–5, Jun. 2015.
[10] P. Bernstein and J. Noudem, "Superconducting magnetic levitation: Principle, materials, physics and models," *Superconductor Sci. Technol.*, vol. 33, no. 3, Jan. 2020, Art. no. 033001.
[11] N. Del Valle, A. Sanchez, E. Pardo, D.-X. Chen, and C. Navau, "Optimizing levitation force and stability in superconducting levitation with translational symmetry," *Appl. Phys. Lett.*, vol. 90, no. 4, Jan. 2007, Art. no. 042503.
[12] K. Ozturk, M. Abdioglu, E. Sahin, S. Celik, H. Gedikli, and B. Savaskan, "The effect of magnetic field distribution and pole array on the vertical levitation force properties of HTS maglev systems," *IEEE Trans. Appl. Supercond.*, vol. 25, no. 4, pp. 1–7, Aug. 2015.
[13] A. M. Campbell, "Forces between arrays of magnets and superconductors," *Superconductor Sci. Technol.*, vol. 15, no. 5, p. 759, Apr. 2002.
[14] K. Liu, W. Yang, G. Ma, L. Quéval, T. Gong, C. Ye, X. Li, and Z. Luo, "Experiment and simulation of superconducting magnetic levitation with REBCO coated conductor stacks," *Superconductor Sci. Technol.*, vol. 31, no. 1, Dec. 2017, Art. no. 015013.
[15] H. Li, Z. Deng, L. Jin, J. Li, Y. Li, and J. Zheng, "Lateral motion stability of high-temperature superconducting maglev systems derived from a nonlinear guidance force hysteretic model," *Superconductor Sci. Technol.*, vol. 31, no. 7, Jun. 2018, Art. no. 075010.
[16] F. Sass, G. G. Sotelo, R. D. A. Junior, and F. Sirois, "H-formulation for simulating levitation forces acting on HTS bulks and stacks of 2G coated conductors," *Superconductor Sci. Technol.*, vol. 28, no. 12, Nov. 2015, Art. no. 125012.
[17] H. Song, O. de Haas, C. Beyer, G. Krabbes, P. Verges, and L. Schultz, "Influence of the lateral movement on the levitation and guidance force in the high-temperature superconductor maglev system," *Appl. Phys. Lett.*, vol. 86, no. 19, May 2005, Art. no. 192506.

[18] N. Del-Valle, A. Sanchez, C. Navau, and D.-X. Chen, "Lateral-displacement influence on the levitation force in a superconducting system with translational symmetry," *Appl. Phys. Lett.*, vol. 92, no. 4, Jan. 2008, Art. no. 042505.
[19] G.-T. Ma, J.-S. Wang, and S.-Y. Wang, "Numerical investigation of the lateral movement influence on the levitation force of the bulk HTS based on a 3-D model," *IEEE Trans. Appl. Supercond.*, vol. 20, no. 3, pp. 924–928, Jun. 2010.
[20] J. Li, H. Li, J. Zheng, B. Zheng, H. Huang, and Z. Deng, "Nonlinear vibration behaviors of high-tc superconducting bulks in an applied permanent magnetic array field," *J. Appl. Phys.*, vol. 121, no. 24, Jun. 2017, Art. no. 243901.
[21] E. Postrekhin, K. Bui Ma, H. Ye, and W.-K. Chu, "Dynamics and relaxation of magnetic stress between magnet and superconductor in a levitation system," *IEEE Trans. Appiled Supercond.*, vol. 11, no. 1, pp. 1984–1987, Mar. 2001.
[22] J. Zheng, H. Huang, S. Zhang, and Z. Deng, "A general method to simulate the electromagnetic characteristics of HTS maglev systems by finite element software," *IEEE Trans. Appl. Supercond.*, vol. 28, no. 5, pp. 1–8, Aug. 2018.
[23] H. Hayashi, H. Ueda, M. Tsuda, A. Ishiyama, and K. Hamajima, "A new type of active-maglev system using YBCO bulk and multiple electromagnets," *IEEE Trans. Appiled Supercond.*, vol. 12, no. 1, pp. 907–910, Mar. 2002.
[24] C. Zhao, Y. Xin, W. Hong, Y. Wen, J. Li, and H. Jin, "Magnetic levitation characteristics of HTS bulk above electromagnets," *IEEE Trans. Appl. Supercond.*, vol. 30, no. 4, pp. 1–5, Jun. 2020.
[25] Y. Wen, Y. Xin, W. Hong, C. Zhao, and W. Li, "Comparative study between electromagnet and permanent magnet rails for HTS maglev," *Superconductor Sci. Technol.*, vol. 33, no. 3, Feb. 2020, Art. no. 035011.
[26] W. Hong, Y. Xin, C. Wang, W. Li, Y. Wen, and C. Zhao, "Study on different YBCO bulk arrangements with a fan-shaped electromagnetic guideway of HTS maglev," *IEEE Trans. Appl. Supercond.*, vol. 30, no. 4, pp. 1–5, Jun. 2020.
[27] W. Hong, Y. Xin, C. Wang, Y. Wen, C. Zhao, and W. Li, "Technical feasibility study of an E-Shaped electromagnetic guideway for HTS maglev," *IEEE Trans. Appl. Supercond.*, vol. 30, no. 6, pp. 1–10, Sep. 2020.
[28] L. Zhao, J. Deng, L. Li, N. Feng, P. Wei, W. Lei, J. Jiang, X. Wang, Y. Zhang, and Y. Zhao, "The influence of inhomogeneous magnetic field over a NdFeB guideway on levitation force of the HTS bulk maglev system," *Phys. C, Supercond. Appl.*, vol. 547, pp. 41–45, Apr. 2018.
[29] Y. Wen, Y. Xin, W. Hong, and C. Zhao, "A force measurement system for HTS maglev studies," *IEEE Trans. Instrum. Meas.*, vol. 69, no. 7, pp. 5018–5026, Jul. 2020.
[30] K. Kajikawa, T. Hayashi, R. Yoshida, M. Iwakuma, and K. Funaki, "Numerical evaluation of AC losses in HTS wires with 2D FEM formulated by self magnetic field," *IEEE Trans. Appiled Supercond.*, vol. 13, no. 2, pp. 3630–3633, Jun. 2003.
[31] Z. Hong, A. M. Campbell, and T. A. Coombs, "Numerical solution of critical state in superconductivity by finite element software," *Superconductor Sci. Technol.*, vol. 19, no. 12, pp. 1246–1252, Dec. 2006.
[32] R. Brambilla, F. Grilli, and L. Martini, "Development of an edge-element model for AC loss computation of high-temperature superconductors," *Superconductor Sci. Technol.*, vol. 20, no. 1, pp. 16–24, Jan. 2007.
[33] M. D. Ainslie, V. M. Rodriguez-Zermeno, Z. Hong, W. Yuan, T. J. Flack, and T. A. Coombs, "An improved FEM model for computing transport AC loss in coils made of RABiTS YBCO coated conductors for electric machines," *Superconductor Sci. Technol.*, vol. 24, no. 4, Jan. 2011, Art. no. 045005.
[34] M. D. Ainslie, W. Yuan, and T. J. Flack, "Numerical analysis of AC loss reduction in HTS superconducting coils using magnetic materials to divert flux," *IEEE Trans. Appl. Supercond.*, vol. 23, no. 3, Jun. 2013, Art. no. 4700104.
[35] V. M. R. Zermeno, F. Grilli, and F. Sirois, "A full 3D time-dependent electromagnetic model for roebel cables," *Superconductor Sci. Technol.*, vol. 26, no. 5, May 2013, Art. no. 052001.
[36] L. Queval, G. G. Sotelo, Y. Kharmiz, D. H. N. Dias, F. Sass, V. M. R. Zermeno, and R. Gottkehaskamp, "Optimization of the superconducting linear magnetic bearing of a maglev vehicle," *IEEE Trans. Appl. Supercond.*, vol. 26, no. 3, pp. 1–5, Apr. 2016.
[37] L. Quéval, K. Liu, W. Yang, V. M. R. Zermeño, and G. Ma, "Superconducting magnetic bearings simulation using an H-formulation finite element model," *Superconductor Sci. Technol.*, vol. 31, no. 8, Jun. 2018, Art. no. 084001.
[38] M. Ainslie, F. Grilli, L. Quéval, E. Pardo, F. Perez-Mendez, R. Mataira, A. Morandi, A. Ghabeli, C. Bumby, and R. Brambilla, "A new benchmark problem for electromagnetic modelling of superconductors: The high-T_c superconducting dynamo," *Superconductor Sci. Technol.*, vol. 33, no. 10, Oct. 2020, Art. no. 105009.
[39] Y. B. Kim, C. F. Hempstead, and A. R. Strnad, "Critical persistent currents in hard superconductors," *Phys. Rev. Lett.*, vol. 9, no. 7, pp. 306–309, Oct. 1962.
[40] D. H. N. Dias, E. S. Motta, G. G. Sotelo, and R. D. Andrade, "Experimental validation of field cooling simulations for linear superconducting magnetic bearings," *Superconductor Sci. Technol.*, vol. 23, no. 7, Jul. 2010, Art. no. 075013.
[41] D. Ruiz-Alonso, T. A. Coombs, and A. M. Campbell, "Numerical analysis of high-temperature superconductors with the critical-state model," *IEEE Trans. Appiled Supercond.*, vol. 14, no. 4, pp. 2053–2063, Dec. 2004.
[42] G.-T. Ma, J.-S. Wang, and S.-Y. Wang, "3-D modeling of high-T_c superconductor for magnetic levitation/suspension application—Part II: Validation with experiment," *IEEE Trans. Appl. Supercond.*, vol. 20, no. 4, pp. 2228–2234, Aug. 2010.

CHAOQUN ZHAO received the M.S. degree in electric machine and electric apparatus from the Shenyang University of Technology, Shenyang, China, in 2013. He is currently pursuing the Ph.D. degree in electrical engineering with Tianjin University, Tianjin, China.

His current research interests include high-temperature superconducting (HTS) maglev, HTS magnetic device and application, and analysis and calculation of electromagnetic field of electric machines.

MARK D. AINSLIE (Senior Member, IEEE) received the B.E. degree in electrical and electronic and the B.A. (Japanese) degree from The University of Adelaide, Australia, in 2004, the M.Eng. degree from The University of Tokyo, Japan, in 2008, and the Ph.D. degree from the University of Cambridge, U.K., in 2012.

From 2012 to 2017, he was a Royal Academy of Engineering Research Fellow of the Bulk Superconductivity Group, University of Cambridge, where he has been an EPSRC Early Career Fellow, since July 2017, as a principal investigator of a project investigating the use of bulk HTS materials in portable high field magnet systems. He has published over 100 articles, and his research interests include the broad range of topics in applied superconductivity in electrical engineering, including superconducting electric machine design, bulk superconductor magnetization, numerical modeling, and interactions between conventional and superconducting materials. In 2011, he was awarded the European Society for Applied Superconductivity (ESAS) Young Researcher's Award in Large Scale Applications, for his Ph.D. work on transport AC loss in high-temperature superconducting (HTS) coils.

YING XIN (Senior Member, IEEE) received the B.S. degree from Tianjin University, Tianjin, China, in 1983, and the Ph.D. degree from the University of Arkansas, Fayetteville, AR, USA, in 1991.

In the past 30 years, he has worked extensively on practical high-temperature superconducting (HTS) materials (bulk, 1G wire, and 2G wire) and power applications of superconductivity. He is currently a Professor with the School of Electrical and Information Engineering, Tianjin University. His current research interests include superconducting fault current limiter, superconducting power cable, superconducting magnetic energy storage (SMES), and HTS maglev.